**Supporting Information for:**

# Mapping the Ion Current Distribution in Nanopore/Electrode Devices

Agnieszka Rutkowska, Joshua B. Edel, Tim Albrecht*

Imperial College London, Department of Chemistry, Exhibition Road, South Kensington Campus, London SW7 2AZ, UK

*** Corresponding author: t.albrecht@imperial.ac.uk**

## 1. Nanopore device microfabrication.

Figure S1 illustrates the device microfabrication protocol as discussed in the experimental section in the main text.

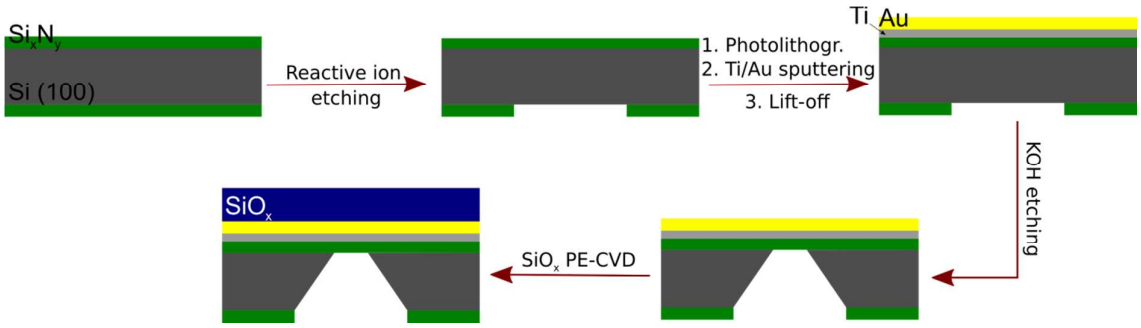


**Figure S1**. Schematic of the device fabrication procedure.

The role of $SiO_x$ film was two-fold. The layer improved the mechanical strength of the membrane. Moreover, the film insulated the microelectrode area and thus reduced the capacitance at the electrode/solution interface as well as Faradaic currents by three orders of magnitude, as measured using cyclic voltammetry (CV) in 1 mM $Fe(CN)_6^{4-}$ in 0.1 M KCl aqueous solution, with a scan rate 100 mV/s versus Ag/AgCl reference electrode.

Specifically, the limiting current due to $Fe(CN)_6^{4-}$ redox reactions was of the order of 1μA and 1 nA for devices without and with the $SiO_x$ layer, respectively. The theoretical value of the limiting current for a nanopore ring electrode with 30 nm height and 15 nm diameter were calculated to be of the order of 1 pA. Higher Faradaic currents at the $SiO_x$-coated devices indicated that the $SiO_x$ film was not free of micro-size pinholes, presumably mostly present around the electrode edges.[1]

## 2. Electrochemical cell set-up.

All electrochemical measurements were performed in a polyether ether ketone cell fabricated in-house, consisted of two reservoirs (*cis* and *trans*) filled with 1 M KCl aqueous solution. The compartments were separated with a nanopore device as shown in Figure 1a in the main text, with the silicon dioxide layer facing up (Figure S1). The 1 mm x 1 mm gold square pad (Figure 1b in the main text) was isolated from the solution. Kwik-cast epoxy was used to keep the sample in place, and to ensure no leakage between the two compartments. A 5 μm tungsten probe was used to create an electrical contact between the metallic nanopore and the external electronic circuit, by micropositioning the needle onto the gold square pad and scratching the $SiO_x$ layer locally over the gold film.

Silver wires with silver chloride coating were prepared in-house and used as quasi-counter and reference electrode (CR), and first working electrode (WE1) in the top (*cis*) and bottom (*trans*) reservoirs, respectively. The metallic nanopore acted as the second WE (WE2).

## 3. Nanopore conductance in the hour-glass model.

The hour-glass nanopore model[2] was adopted to calculate the theoretical diameter of the solid-state metallic nanopores with the nanopore length, $l$, 215 nm, based on the nanopore resistance (Figure S2):

$$R_{\text{hyp}} + \frac{2\rho}{\pi D} < R < R_{\text{hyp}} + \frac{\rho}{D} \qquad \text{(S1)}$$

where $R_{\text{hyp}}$ and $R$ are the resistance of an hour-glass nanopore, and the full measured resistance between two electrodes, CR and WE1, respectively, $\rho$ is the solution resistivity, and $D$ is the outer diameter of the nanopore. $R_{\text{hyp}}$ is defined as:

$$R_{\text{hyp}} = \frac{2\rho}{\pi d}\frac{\sin\alpha}{1-\cos\alpha}\arctan\left(\frac{\sqrt{D^2-d^2}}{d}\right) \qquad \text{(S2)}$$

where $d$ is the internal diameter of the nanopore in its narrowest point, and $\alpha$ is the asymptotic opening angle of the hyperboloid:

$$\sin^2\alpha = \frac{D^2-d^2}{l^2+D^2-d^2} \qquad \text{(S3)}$$

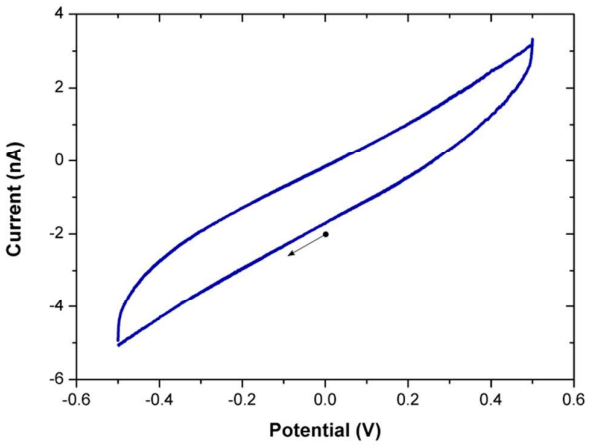


**Figure S2.** Transmembrane ionic current trace in 1 M KCl and at a scan rate of 100 mV/s with the nanopore electrode (WE2) switched off. The arrow indicates the initial scan direction.

## 4. Ionic current at the counter/reference electrode.

Figure S3 shows the contour plot of CR ionic current, $I_{\text{CR}}$, as a function of both potentials, $E_1$ and $E_2$, at a steady state in 1 M KCl. $I_{\text{CR}}$ was calculated based on the Kirchoff's law: $\sum_{i=1}^{n} I_i = 0$, where $I_i$ corresponds to the ionic current at the WE1, WE2 and CR (*c.f.* Figure 2a and b for the values of $I_1$ and $I_2$, respectively). The $I_{\text{CR}}$ range remains in the order of ± 1 nA, hence, has a negligible effect on the total current flow, taking place predominantly between WE1 and WE2, as discussed in the main text.

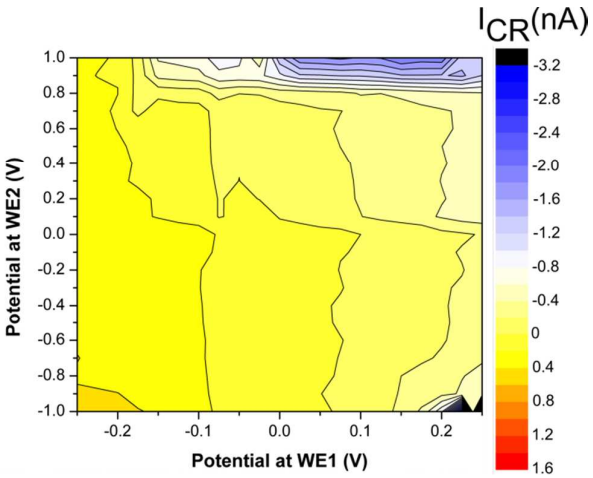


**Figure S3.** Ionic current at CR in 1 M KCl at the steady state.

## 5. Electric equivalent circuit of the three-electrode set-up.

Figure S4 shows a simple electric equivalent circuit representative of the electrochemical cell of interest.[3] The idea behind this approach is that the currents flowing through the three electrodes CR, WE1 and WE2 have to balance; for example, reduction on one electrode must be counter-balanced by oxidation on the other two and so forth. Formally, this may be represented by a node or summing point 'sp', where all currents add up to zero (Kirchhoff's 1st Law). The current detected at WE1 is then calculated from the admittance of the WE1/sp circuit branch and the potential drop between sp and WE1, $E_{1sp}$ (in Laplace space). The derivation of the equations for the currents is based on standard circuit theory and will not be repeated in detail here. Some comments are still appropriate to indicate the general route towards the solution. Note that the potential drop between sp and CR, $E_{spCR}$, is dependent on current flow through WE1 and WE2. The potential difference between WE1 and CR (which is an experimental parameter), $E_{1CR}$, is the sum of $E_{spCR}$ and $E_{1sp}$; the same considerations apply to $E_{2CR}$. The admittance $Y_i$ for each circuit branch, $Y_{spCR}$, $Y_{1sp}$ and $Y_{2sp}$, and the potential differences between sp and the respective electrode, $E_{spCR}$, $E_{1sp}$ and $E_{2sp}$, are then entered into Kirchhoff's 1st Law to obtain an expression for $E_{1sp}$ as a function of all the other transfer functions $Y_i$ and potentials $E_{1CR}$ and $E_{2CR}$. In conjunction with $Y_{1sp}$, this can then be used to calculate the current $I_{1sp}$, which in the present picture is the current detected at WE1, $I_1$. What remains is to use the appropriate input functions for $E_{1CR}$ and $E_{2CR}$ (in Laplace space), depending on the simulation scenario, e.g. $\tilde{E}_{1CR} = E_1/s$ and $\tilde{E}_{2CR} = E_2/s$ for constant potentials $E_1$ and $E_2$ ($s = i\omega$ is the (imaginary part of the) Laplace parameter), and calculate the inverse Laplace transform to obtain the current in the time domain (potentially neglecting time-dependent transients for the steady-state case). The resulting expressions are rather laborious, especially for more complex input function. Hence, we used MathCad 13 (Mathsoft) to

obtain the analytical expressions; their accuracy was in turn confirmed by numerical calculations using Spice.

The rationale behind the circuit components is as follows. Since Ag/AgCl electrode is close to ideal nonpolarizable electrode, the charge transfer resistance, $R_{ct}$, at CR and WE1, is very low or, ideally, 0; thus, capacitive charging is negligible. This leaves the solution resistance components, (i) $R_{s1}$, and (ii) $R_{s2}$ and $R_{s2"}$ for CR and WE1, respectively. For WE1, the solution resistors are in series with the pore resistor, $R_{pore}$, and membrane capacitance, $C_{mem}$. The charge transfer properties of WE2 depend on $R_{ct}$, i.e. on the potential applied, $E_2$. Hence, its solution resistance, $R_{s2'}$, is in series with the $R_{ct}$ and double layer capacitance, $C_{dl}$. Note that, in the limit of $R_{ct} \rightarrow \infty$ in steady-state, WE2 does not pass any currents and the remaining part of the equivalent circuit simply represents a conventional two-electrode setup.

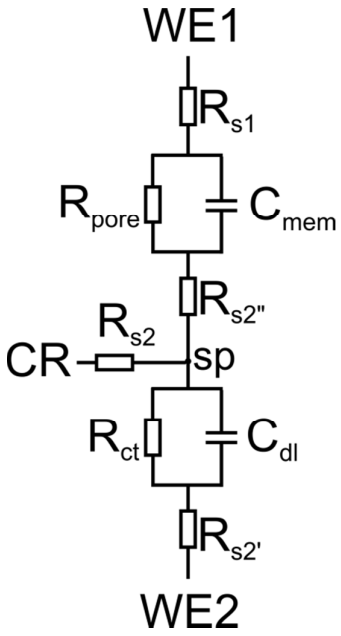


**Figure S4.** Electric equivalent circuit model. See main text for detail discription of the circuit components.

## 6. Verification of the theoretical model of ionic current distribution in the cell.

Figure S5 shows the error contour plot of the fitting procedure of the simulated ionic current at the WE1, $I_{1sim}$, to the experimental results, $I_{1exp}$ (see main text for detailed description). The error was calculated using the least squares method with $R_{s2}$ and $R_{pore}$ as the fitting parameters:

$$\text{Error}(R_{pore}, R_{s2}) = \frac{\sqrt{\sum_{i=1}^{N}(I_{1exp} - I_{1sim})^2}}{N}$$

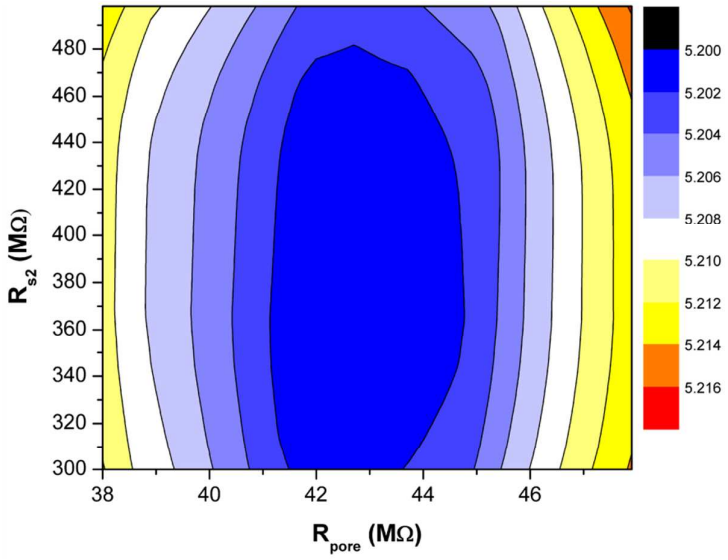


**Figure S5.** 2D error surface for the least square fit of eq. (1) to steady-state experimental data with $R_{s2}$ and $R_{pore}$ as fitting parameters. The best fit was obtained for $R_{pore}$ = 42.5 MΩ and $R_{s2}$ = 368 MΩ.

## 7. Simulated contour plots of $I_1(E_1,E_2)$, when $E_1$ is ramped at constant $E_2$

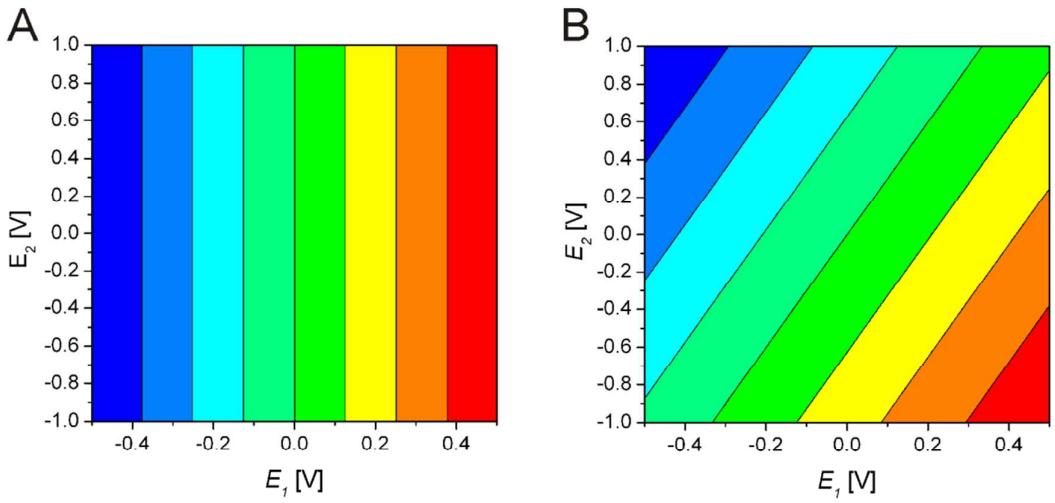


**Fig. S6**: Simulated contour plots of $I_1(E_1,E_2)$ when $E_1$ is ramped from -0.5 V to +0.5 V with 0.1 V/s at constant $E_2$, based on eq. 1. Currents in arbitrary units range from negative (blue) to positive values (red). Limits of very large and very small (constant) $R_{ct}$. A: $R_{ct} >> R_{pore}$, $I_1$ is independent of $E_2$ (surface charge effects are not included in the model). B: $R_{ct} << R_{pore}$, $I_1$ is strongly affected by $E_2$ and the potential drop across the pore depends on both $E_1$ and $E_2$. Note that the colors stand for current ranges, not for single values. Thus, equally spaced contour lines represent linear changes of $I_1$ with $E_1$ and $E_2$, respectively. Interestingly, the experimental data in fig. 3 (main text) can be seen as in between these two limits. The main difference is that $R_{ct}$ changes with $E_2$ (and $E_1$), which is not included in the model above, cf. also fig. 2C.

REFERENCES

[1] Mattox, D.,M. *Handbook of Physical Vapor Deposition (PVD) Processing*, Elsevier **2010**.

[2] Kowalczyk, S. W.; Grosberg, A. Y.; Rabin, Y.; Dekker, C. *Nanotechnology*, **2011**, 22, 315101.

[3] Albrecht, T. *ACS Nano*, **2011**, 5, 6714.